Earth and Planetary Science Letters 523 (2019) 115706

Contents lists available at ScienceDirect

Earth and Planetary Science Letters

www.elsevier.com/locate/epsl

Isotopic evidence for a young lunar magma ocean

Lars E. Borg *, Amy M. Gaffney, Thomas S. Kruijer, Naomi A. Marks, Corliss K. Sio, Josh Wimpenny

Nuclear and Chemical Sciences Division, Lawrence Livermore National Laboratory, Livermore, CA 94550, USA

ARTICLE INFO

Article history:
Received 2 February 2019
Received in revised form 1 July 2019
Accepted 7 July 2019
Available online xxxx
Editor: F. Moynier

Keywords:
Moon
age
magma ocean
Sm-Nd isotopes
crust
mantle

ABSTRACT

Mare basalt sources and ferroan anorthosite suite cumulates define a linear array on a $^{146}Sm/^{144}Nd$ versus $^{142}Nd/^{144}Nd$ isochron plot demonstrating these materials were derived from a common reservoir at $4336^{+31}/_{-32}$ Ma. The minimum proportion of the Moon that was in isotopic equilibrium at this time is estimated to be 1-3% of its entire volume based on the geographic extent from which the analyzed samples were collected and the calculated depths from which the samples were derived. Scenarios in which large portions of the Moon were molten to depths of many hundreds of kilometers are required to produce the observed Sm-Nd isotopic equilibrium between the mantle and crustal rocks at 4.34 Ga. This is a consequence of the fact that limited heating of a solid Moon above the blocking temperature of the Sm-Nd isotopic system is insufficient to diffusively homogenize radiogenic Nd throughout the mantle and crust. There are three scenarios that might account for global-scale isotopic equilibrium on the Moon relatively late in Solar System history including: (1) Sm-Nd re-equilibration of a solid Moon resulting from widespread melting in response to mantle overturn or a very large impact, (2) early accretion of the Moon followed by delayed cooling due to the presence of an additional heat source that kept a large portion of the Moon molten until 4.34 Ga, or (3) late accretion of the Moon followed by rapid cooling of the magma ocean late in Solar System history. Neither density-driven overturn of the mantle, nor a large impact, are likely to homogenize the mantle and crust to the extent required by the Sm-Nd isochron. Likewise, secondary heating mechanisms, such as tidal heating or radioactive decay, are not efficient enough to keep the Moon molten to the depth of the mare basalt source regions for many tens to hundreds of millions of years. Instead, the age of equilibrium between such a compositionally diverse set of rocks, produced on a global scale, likely records the time of primordial solidification of the Moon from a magma ocean. This scenario accounts for both the petrogenetic characteristics of lunar rock suites, as well as their Sm-Nd isotopic systematics. It is supported by the preponderance of ~4.35 Ga ages obtained for other hypothetical magma ocean crystallization products, such as ferroan anorthosite suite rocks and K, REE, and P enriched cumulates that are thought to represent flotation cumulates of the magma ocean and the last vestiges of magma ocean solidification, respectively.

1. Introduction

Numerous attempts to determine the time of formation of the Moon (and Earth) by dating individual lunar rocks have yielded ambiguous results. This stems from the fact that isotope clocks only determine the age when individual rocks, or suites of rocks, were produced. In order for these ages to constrain the time of formation of a planetary body such as the Moon, the rocks must have well-defined geologic links to the processes that formed the body. Thus, there are two bases to legitimately question any geochronologic determination for the age of the Moon. The first is whether the age accurately defines a geologic event, and the second is whether the event is primordial solidification. These issues have stymied the development of a consensus for the age of the Moon.

The Lunar Magma Ocean (LMO) model provides a petrogenetic framework within which to interpret the ages of lunar rocks. It was initially developed at the dawn of the Apollo sample analysis program (Smith et al., 1970; Wood et al., 1970) and has been refined continuously ever since (Snyder et al., 1992; Elkins-Tanton et al., 2011). In this model, the Moon accreted from the debris of a Giant Impact between the proto-Earth and another large body (Hartmann and Davis, 1975), resulting in large-scale melting of the Moon followed by cooling and primordial solidification. As the molten body cooled, crystallization produced a sequence of cumulate rocks. The first cumulates to form con-

* Corresponding author.
E-mail address: borg5@llnl.gov (L.E. Borg).

https://doi.org/10.1016/j.epsl.2019.07.008
0012-821X/

tained the minerals olivine and low Ca-pyroxene, which sank to the base of the LMO. The next cumulates to form contained olivine, pigeonite, and clinopyroxene, which also sank. Anorthositic (Ca-rich) plagioclase crystallized next from a relatively dense iron-rich liquid. As a consequence of the density difference between plagioclase and remaining liquid, the plagioclase floated, forming the anorthositic lunar crust. Subsequent crystallization produced clinopyroxene-bearing cumulates rich in ilmenite, followed by a residuum called urKREEP (Warren and Wasson, 1979) that contains high abundances of potassium (K), rare earth elements (REE), and phosphorous (P) that were mostly excluded from the previously formed minerals. These various LMO cumulates were subsequently melted to produce the intrusive magmas of the Mg-suite and extruded on the surface in the form of mare basalts.

The short-lived Sm-Nd isotopic system, in which ^{146}Sm decays to ^{142}Nd with a half-life of 103 ± 5 Ma, provides a mechanism to date the formation of the LMO cumulates. This approach was developed by Nyquist et al. (1995), who obtained an age of approximately 4.33 Ga for the formation of the LMO cumulate sources of the mare basalts. They also discovered that high neutron fluences near the lunar surface required large corrections to be made on the ^{147}Sm/^{144}Nd, ^{143}Nd/^{144}Nd, and ^{142}Nd/^{144}Nd ratios measured on many samples. The methods employed by the original study of Nyquist et al. (1995) have been repeated several times (Rankenburg et al., 2006; Boyet and Carlson, 2007; Brandon et al., 2009; McLeod et al., 2014), and although the isotopic measurements have become more precise and neutron corrections have become more sophisticated, the ~4.33 Ga result has remained essentially constant. However, despite the reproducibility of the measurement, the significance of the ^{146}Sm-^{142}Nd age of the mare basalt sources has remained controversial.

The Sm-Nd age determined for the mare basalt source regions has been interpreted in several ways. Nyquist et al. (1995) originally interpreted the age to record primordial solidification of the LMO. This interpretation is problematic because more ancient ages have been determined for some lunar samples. For example, a model age for the formation of urKREEP, the last material to form from the LMO, of >4.51 Ga was recently calculated from U-Pb ages and Lu-Hf isotopic systematics of lunar zircons (Barboni et al., 2017). If this zircon Hf model age is correct, then the ~4.33 Ga age determined for the mare basalt sources cannot represent primordial solidification of the LMO. Another interpretation of the ~4.33 Ga age is that it represents re-equilibration of the mare basalt source regions significantly after they formed in the LMO. Re-equilibration of the mare basalt source regions has been postulated to have occurred as a result of density driven overturn of the LMO (Borg et al., 2011) or regional melting resulting from a large impact (McLeod et al., 2014). Finally, the young age could, in principle, reflect delayed cooling of the LMO as a result of the presence of another heat source, such as radioactive decay (Shearer et al., 2006) or tidal heating (Garrick-Bethell et al., 2010; Meyer et al., 2010).

Fortunately, petrogenetic, geochemical, and thermal models of solidification of the LMO make three predictions that can be used to elucidate whether the mare basalt Sm-Nd age records primordial LMO solidification or post-LMO re-equilibration. First, all LMO cumulates should have formed within a few million years of one another (Elkins-Tanton et al., 2011). Second, all LMO cumulates should have been derived from a common source region with a homogeneous isotopic composition, such that all LMO cumulates should form in isotopic equilibrium (e.g., Smith et al., 1970; Wood et al., 1970; Snyder et al., 1992; Elkins-Tanton et al., 2011). Finally, LMO cumulates should be distributed globally. These predictions are tested below using new Sm-Nd isotopic data obtained on a large set of mare basalts and Ferroan Anorthosite Suite (FAS) rocks.

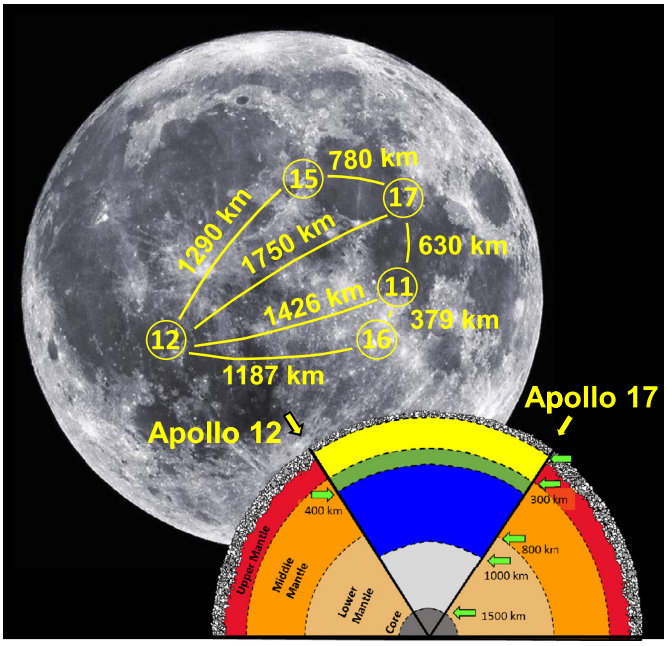

Fig. 1. Position of Apollo landing sites depicting geographic distance between samples. Yellow, green, and blue areas of inset represents source regions of basalts based on melting depths proposed in the literature. Volume of Moon represented by basalt source regions analyzed here is calculated to represent 0.8 (yellow field), 1.0 (green + yellow fields), or 2.9 (blue, green, and yellow fields) volume percent of Moon depending on depth of mare basalt source regions. Note that no samples from Apollo 14 were analyzed in this investigation. (For interpretation of the colors in the figure(s), the reader is referred to the web version of this article.)

2. Sample selection and characterization

To evaluate whether the mare basalt source regions formed contemporaneously from a common reservoir, and whether this reservoir was global in scale, we have measured the Sm and Nd isotopic compositions of 30 mare basalts selected from the Apollo 11, 12, 15, 17 and lunar meteorite sample suites. These data are compared to similar data we have obtained on FAS crustal cumulates, which are hypothesized to be flotation cumulates of the LMO, in order to further evaluate the global extent of Sm-Nd isotopic equilibrium on the Moon. Not only does this investigation double the number of basalt samples analyzed for ^{142}Nd isotope compositions, it significantly increases the diversity in the sample set by selecting rocks that were collected in distal geographic locations (Fig. 1), that represent both mantle and crustal lithologies, and that span virtually all of the compositional variation observed in the lunar basalt suite (see Supplementary Material).

The suite of basalt samples analyzed in this investigation demonstrates significant mineralogical diversity and is composed of ilmenite basalts, olivine basalts, and pigeonite basalts (see Supplementary Material). Using the scheme of Neal et al. (1994), and Ti, Al, and K abundances measured in this investigation, the basalts are classified as high-Ti/low-K, high-Ti/high-K, low-Ti, high-Al, and very high-K. Thus, 5 of the 6 classes of basalts defined by Neal et al. (1994) are represented in this study. Limited mass and absence of age determinations resulted in the omission of the very low-Ti basalts from this study. Major and trace element compositions confirm that the samples represent a broad spectrum of lunar basalt compositions (see Supplementary Material), spanning most of the compositional range observed in the Apollo collection (Fig. 2). In fact, one sample, 15388, which had not been analyzed previously, defines a unique position on Fig. 2 (upper right) that expands the known compositional range of the mare basalts.

The main objective of this investigation is to define a ^{146}Sm-^{142}Nd whole rock isochron with as much spread in ^{147}Sm/^{144}Nd

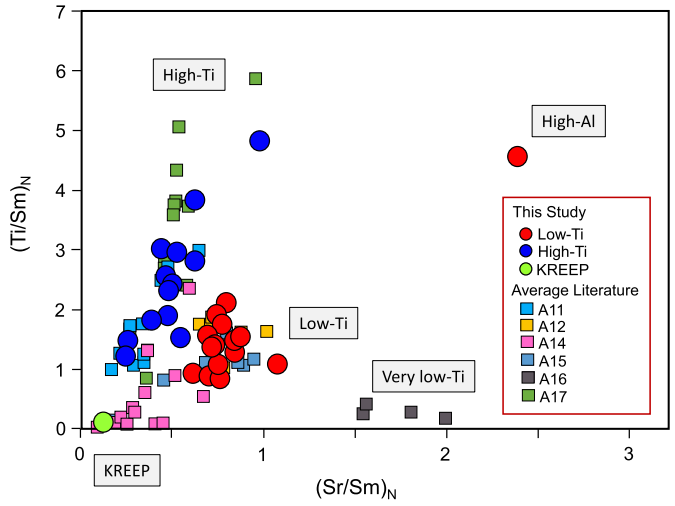

Fig. 2. Compositional variation of samples analyzed in this investigation. Compositions of samples analyzed in this study (circles) compared to average compositions determined for Apollo basalts (squares). Ratios normalized to elemental abundances in hand-picked green glass (sample 15426) analyzed in this investigation and presented in the Supplementary Material.

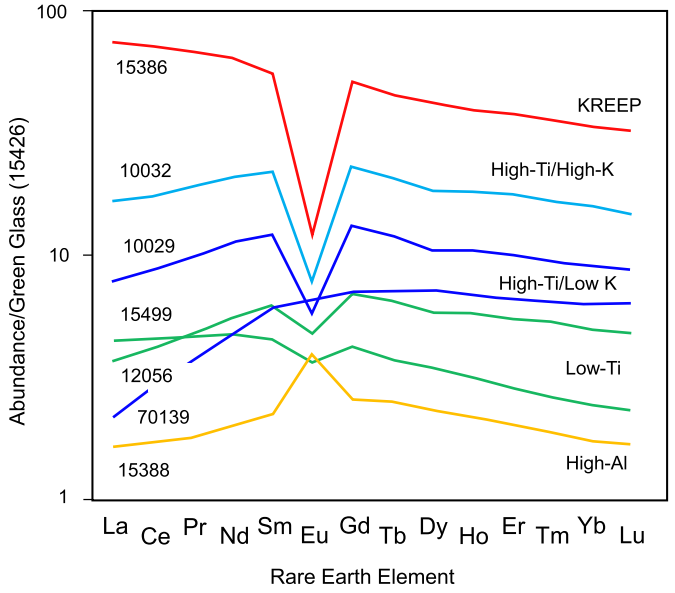

Fig. 3. REE patterns of representative mare basalts demonstrating variations in the sample suite as well as the independence of the REE patterns from the mineralogical and geochemical classification schemes used to characterize the basalts (see text). Data normalized to 15426 green glass analyzed in this investigation. Green glass is used for normalization because it has nearly chondritic proportions of REE and was analyzed contemporaneously with the samples minimizing analytical bias.

ratios as possible using the most diverse and geographically extensive suite of samples available. As a consequence, samples were also selected for isotopic analysis based on their REE patterns (Fig. 3). The REE data are normalized to hand-picked Apollo 15 green glass spherules from sample 15426 analyzed in the course of this study (see Supplementary Material). The use of REE patterns as a sample selection tool is based on the observation that the REE patterns of the rocks are not well correlated with their classifications based on major elements, such as Ti, K, and Al, or their mineral modes. This is illustrated on Fig. 3 by differing REE patterns for individual samples of low-Ti basalts (green lines), as well as high-Ti basalts (dark-blue lines). The basalts have patterns that range from light-REE enriched to strongly LREE-depleted relative to Apollo 15 green glass. The extent of LREE depletion or enrichment observed in the bulk samples generally correlates with the $^{147}Sm/^{144}Nd$ ratios calculated for the basalt sources (see below). Thus, the REE patterns serve as a reasonable proxy for $^{147}Sm/^{144}Nd$ in the basalt sources and ensure maximum spread of the data on the ^{146}Sm-^{142}Nd isochron.

3. Analytical techniques

Samples analyzed for Sm, Nd, and Hf isotopic compositions were washed in distilled H_2O prior to crushing in a sapphire mortar and pestle. The samples were weighed and then digested in a class 100 clean laboratory using Parr bombs and HF and HNO_3 acids following methods presented in Gaffney and Borg (2014). Once fully digested, the sample solutions were split into A and B fractions. A mixed Sm-Nd isotopic tracer was added to the A fraction which was then used to obtain Hf isotope compositions and Sm-Nd concentrations. The Nd and Sm isotopic compositions were determined from the B fraction.

The chemical separation and mass spectrometry procedures used in this investigation are published in Connelly et al. (2006), Gaffney and Borg (2014), and Borg et al. (2016) and discussed in detail in the Supplementary Material. In brief, high field strength elements (HFSE) were separated from the basalt matrix in the A fraction using cation resin and HCl-HF acids, whereas Hf was purified from most other HFSE using DGA resin and various combinations of HNO_3, HF, and HBO_3 acids. Samarium and Nd were purified from the matrix cut from the first column using cation resin and HCl acids. The two REEs were purified from one another using a pressurized column loaded with cation resin in the ammonia form and α-HIBA acid. Procedural blanks were 15 pg Hf, 8 pg Sm, and 15 pg Nd.

Hafnium from the A fraction was run on a Nu-Plasma HR at LLNL using the standard-sample bracketing technique. The JMC 475 Hf isotopic standard was used as the standard. Analytical runs consisted of 30 cycles of 10 s integrations with a beam intensity of 5.5 V of ^{180}Hf (10^{11} Ω amplifier resistors). Potential interfering elements were monitored at ^{182}W, ^{175}Lu, and ^{172}Yb and were negligible. Samarium and neodymium from the A fraction were measured on the Triton thermal ionization mass spectrometer at LLNL. Samarium was run in static mode at 0.2-0.5 V of ^{149}Sm for 100 cycles of 8 s integrations. Interferences were monitored at ^{155}Gd and ^{146}Nd and were negligible. Samarium was corrected for instrument induced mass bias using $^{147}Sm/^{152}Sm = 0.560828$. Neodymium was also measured on the LLNL Triton using a static acquisition routine. It was run at 4-6 V (10^{11} Ω amplifier resistors) for 200 cycles of 8 s integrations. Interferences were monitored at ^{140}Ce and ^{149}Sm. Neodymium was corrected for instrument induced mass bias using $^{146}Nd/^{144}Nd = 0.7219$. Hafnium isotopic compositions, Sm and Nd concentrations, as well as $^{147}Sm/^{144}Nd$ and $^{143}Nd/^{144}Nd$ isotopic ratios for the mare basalts are presented in the Supplementary Material.

The isotopic compositions of Sm and Nd were measured in the B fraction. The chemical separation was based on the same two column procedures outlined above that involved an initial cation column and HCl acids, followed by a second pressurized column loaded with cation resin that had been converted to the ammonia form and α-HIBA acid. The only difference between the chemical separation procedures used for the isotope dilution measurements and isotopic composition measurements is that the Nd fraction was passed through the pressurized α-HIBA column twice to further purify Nd from Ce. Samarium was run as outlined above except with larger signal intensities, up to 3 V of ^{149}Sm, and longer analytical durations of 200 to 300 cycles. Neodymium was run using a two-cycle dynamic routine for 540 ratios of 8 s integrations. The $^{142}Nd/^{144}Nd$ and $^{148}Nd/^{144}Nd$ ratios are dynamic ratios, whereas $^{143}Nd/^{144}Nd$, $^{145}Nd/^{144}Nd$, and $^{150}Nd/^{144}Nd$ are obtained

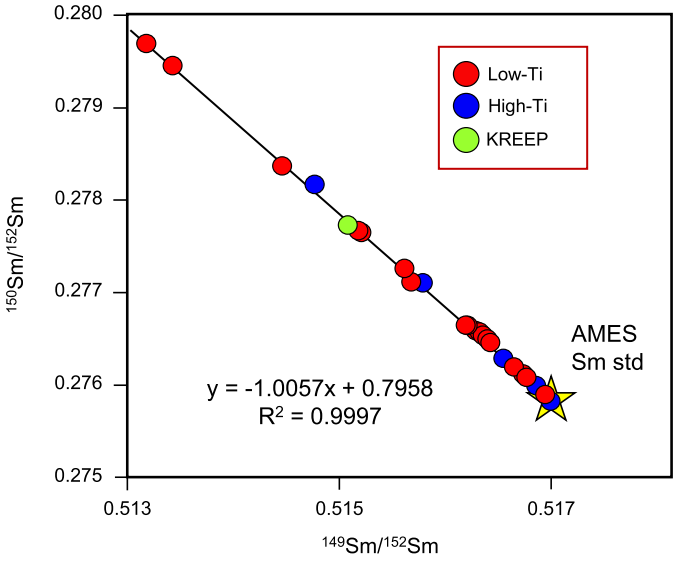

Fig. 4. Samarium isotope compositions of mare basalts. Plot illustrates magnitude of isotopic shifts in Sm due to neutron capture.

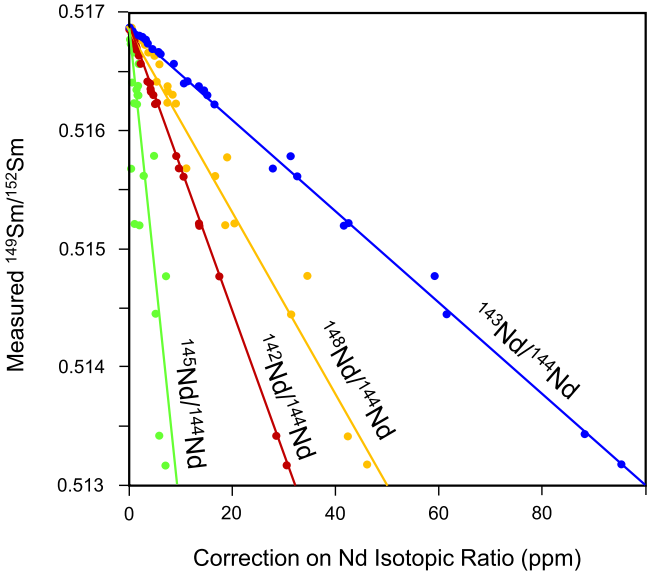

Fig. 5. Neutron capture corrections on Nd isotopes. Plot of $^{149}Sm/^{152}Sm$ measured in the samples versus the correction on the measured $^{142}Nd/^{144}Nd$ (red), $^{143}Nd/^{144}Nd$ (blue), $^{145}Nd/^{144}Nd$ (green), and $^{148}Nd/^{144}Nd$ ratios (yellow) of the mare basalts.

statically. Individual filaments were often run multiple times so that ratios from all cycles were averaged. The Nd and Sm isotopic compositions measured for the mare basalts are presented in the Supplementary Material.

4. Neutron irradiation corrections

The isotopic compositions of Sm, Nd, and Hf are modified by the capture of both epithermal and thermal neutrons produced in the lunar regolith as a result of interaction with galactic cosmic rays. The isotopic composition of Hf is predominantly affected by epithermal neutrons, whereas the isotopic composition of Sm and Nd are modified more by thermal neutrons. Fig. 4 illustrates the effects of neutron capture on ^{149}Sm producing ^{150}Sm. Note the data pass though the terrestrial AMES Sm standard and define a slope of −1.0057 which is essentially identical to the theoretical slope of −1 predicted for neutron capture.

Isotopic data were corrected for neutron capture using the procedure outlined by Gaffney and Borg (2014). This model uses the measured isotopic composition of Hf and Sm in individual samples in combination with the measured REE abundances of the rocks to estimate the fluences of epithermal and thermal neutrons that interacted with that sample. It is assumed that pre-irradiation Hf and Sm isotopic composition of the samples are the same as that measured for JMC 475 Hf and AMES Sm standards. The pre-irradiation Nd isotopic composition of each sample was calculated from the measured Nd isotopic compositions using the modeled thermal and epithermal neutron fluences, the thermal neutron capture cross sections and resonance integrals tabulated by Sprung et al. (2010, 2013), and equation A2 of Nyquist et al. (1995).

The magnitude of correction on each Nd isotopic ratio measured for the mare basalts is plotted against their $^{149}Sm/^{152}Sm$ isotopic composition (Fig. 5) in order to illustrate the size of the neutron capture correction, as well as to provide a means to correct the Nd isotopic compositions of two samples (15475 and 62237) for which Hf isotopic compositions were not measured. Note that the data arrays are not perfectly linear as a result of variable proportions of epithermal to thermal neutron fluences experienced by each sample. Nevertheless, the measured $^{149}Sm/^{152}Sm$ ratio provides a relatively good proxy for the correction on the Nd isotopic compositions because both Sm and Nd are minimally modified by epithermal neutrons. From this plot it is apparent that about half of mare basalts have neutron fluence corrections on $^{142}Nd/^{144}Nd$ that are less than the reported analytical uncertainty of 6 ppm (Fig. 5).

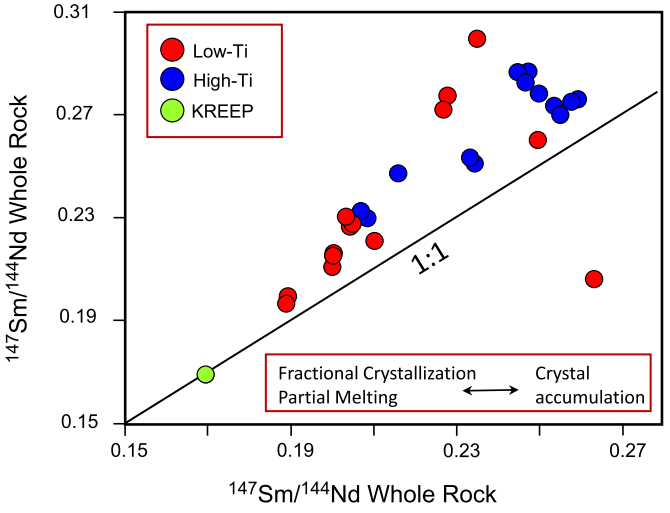

Fig. 6. Comparison of measured $^{147}Sm/^{144}Nd$ ratios of mare basalts with calculated $^{147}Sm/^{144}Nd$ ratios of their sources illustrating why the measured $^{147}Sm/^{144}Nd$ ratios cannot be substituted for $^{147}Sm/^{144}Nd$ ratios calculated for the source regions on the ^{146}Sm-^{142}Nd isochron plot.

5. Calculation of the mare basalt ^{146}Sm-^{142}Nd isochron

The approach and mathematical algorithms used to obtain an age for the formation of the mare basalt source regions are discussed in detail in Borg et al. (2016). Briefly, the measured $^{142}Nd/^{144}Nd$ ratios of the mare basalts are plotted against the $^{147}Sm/^{144}Nd$ ratios calculated for their sources to obtain the initial $^{146}Sm/^{144}Sm$ ratio of the reservoir from which the mare basalt source regions formed (Fig. 7). To do this the $^{147}Sm/^{144}Nd$ ratios of the mare basalt sources must first be calculated from the crystallization ages, as well as the $^{147}Sm/^{144}Nd$ and $^{143}Nd/^{144}Nd$ ratios of the samples presented in the Supplementary Material using Equation (1):

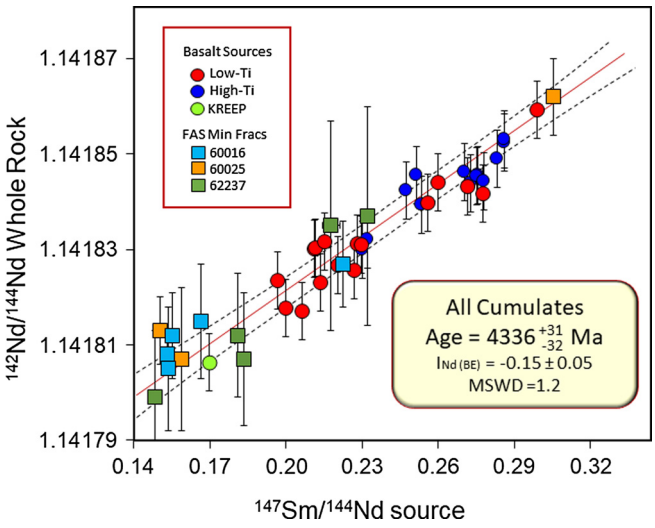

Fig. 7. ^{146}Sm-^{142}Nd isochron diagram of lunar mantle and crustal cumulates. Isochron calculated using data from mare basalt source regions and mineral fractions from anorthositic samples 60016 (Marks et al., 2014b), 60025 (Borg et al., 2011), and 62237 (Sio and Borg, 2018). The regression (solid red line) through the data yields an age of $4336^{+31}/_{-32}$ Ma. Error envelope (dashed lines) represents uncertainty on regression which is ±10 Ma. An age of $4331^{+35}/_{-37}$ Ma is calculated from the basalt data alone (regression not shown). Error bars are 2× standard deviation of replicate analysis on Nd standard or 2× standard error of individual mass spectrometry runs, whichever is larger.

$$\left(\frac{^{147}\mathrm{Sm}}{^{144}\mathrm{Nd}}\right)^{S} = \frac{[(\frac{^{143}\mathrm{Nd}}{^{144}\mathrm{Nd}})^{M3} - (\frac{^{143}\mathrm{Nd}}{^{144}\mathrm{Nd}})^{SSI} - (\frac{^{147}\mathrm{Sm}}{^{144}\mathrm{Nd}})^{Ch}(e^{\lambda^{147}T_0} - e^{\lambda^{147}T_1}) - (\frac{^{147}\mathrm{Sm}}{^{144}\mathrm{Nd}})^{M1}(e^{\lambda^{147}T_2} - 1)]}{(e^{\lambda^{147}T_1} - e^{\lambda^{147}T_2})} \quad (1)$$

The measured Nd isotopic composition of the basalt is $(\frac{^{143}\mathrm{Nd}}{^{144}\mathrm{Nd}})^{M3}$, $(\frac{^{143}\mathrm{Nd}}{^{144}\mathrm{Nd}})^{SSI}$ is the initial Nd isotopic composition of the solar system of 0.506674, $(\frac{^{147}\mathrm{Sm}}{^{144}\mathrm{Nd}})^{Ch} = 0.1967$, and $(\frac{^{147}\mathrm{Sm}}{^{144}\mathrm{Nd}})^{M1}$ is the value measured for each mare basalt sample. $T_0 = 4567$ Ma, T_2 = crystallization age of rock, and T_1 = age of differentiation of the source region.

The age of the source region, T_1, is then obtained using the Equation (2):

$$T_1 = 4567 - \left(\frac{1}{-\lambda^{146}}\right)\ln\left[\frac{m}{(\frac{^{146}\mathrm{Sm}}{^{144}\mathrm{Sm}})^{SSI}(\frac{^{144}\mathrm{Sm}}{^{147}\mathrm{Sm}})^{Std}}\right] \quad (2)$$

The slope of the isochron is m. The slope is determined by linear regression of the data on the isochron plot. The value for $(\frac{^{146}\mathrm{Sm}}{^{144}\mathrm{Sm}})^{SSI}$ is 0.0828 ± 0.0044 (Marks et al., 2014a) and the value for $(\frac{^{144}\mathrm{Sm}}{^{147}\mathrm{Sm}})^{Std}$ is the present-day ratio determined on the AMES Sm standard = 0.202419. The age is calculated relative to Pb-Pb age of CAIs of 4567 Ma (Connelly et al., 2012). The value for λ is calculated from the ^{146}Sm half-life of 103 ± 5 Ma. This half-life is adopted here because Marks et al. (2014a) demonstrated that the shorter half-life determined by Kinoshita et al. (2012) fails (underestimates) to reproduce the ^{147}Sm-^{143}Nd ages measured on fractions from which ^{146}Sm-^{142}Nd isochrons have also been determined.

Both the ^{147}Sm/^{144}Nd ratio of the mare basalts sources and the age of formation of the source region (T_1) are calculated from Eqs. (1) and (2) iteratively. In the first iteration, ^{147}Sm/^{144}Nd of the basalt sources is calculated using Eq. (1) assuming they were produced at 4567 Ma (i.e. $T_1 = 4567$ Ma). Next, an age for basalt source formation is calculated using Eq. (2) from the slope obtained by plotting the ^{147}Sm/^{144}Nd calculated for the mare basalt sources against the ^{142}Nd/^{144}Nd measured for the basalts. This calculated age is younger than 4567 Ma and is substituted into Eq. (1) for T_1 and new ^{147}Sm/^{144}Nd ratios for the mare basalts sources are obtained. Note that the ^{147}Sm/^{144}Nd ratios calculated for the mare basalt sources are larger than those measured for the bulk rocks and fall above the 1:1 (Fig. 6). This reflects the fact that Sm behaves more compatibly than Nd during partial melting. In addition, the data plotted on Fig. 6 are scattered because lunar basalts have been produced by variable degrees of partial melting from mineralogically diverse sources, and have undergone varying extents of both fractional crystallization and crystal accumulation. Thus, the ^{147}Sm/^{144}Nd ratio measured for the basalts cannot be substituted for the ^{147}Sm/^{144}Nd ratio calculated for their sources on the isochron diagram.

6. Results

The Sm-Nd isotopic data for the mare basalt sources are presented in the Supplementary Material and plotted on a ^{146}Sm-^{142}Nd isochron (Fig. 7). Despite the fact that the basalts were selected to maximize composition diversity and geographic distance, all mare basalts lie within error of a single isochron regression. The age records when mare basalt source regions were in isotopic equilibrium and is calculated to be $4331^{+35}/_{-37}$ Ma. Note that the errors calculated on the isochron ages presented here includes ~5% uncertainty on the ^{146}Sm half-life reported by Meissner et al. (1987) which accounts for ~22 Ma of the stated uncertainty. Although the calculated age is in excellent agreement with previous ^{146}Sm-^{142}Nd isochron ages determined on mare basalts (Nyquist et al., 1995; Rankenburg et al., 2006; Boyet and Carlson, 2007; Brandon et al., 2009; McLeod et al., 2014), it is impossible to directly compare the data from the various studies because each has adopted a slightly different approach to measure ^{142}Nd/^{144}Nd and correct for neutron capture on Nd. This effects the y-intercept, but not the slope, of the isochron.

The significance of the ^{146}Sm-^{142}Nd isochron must be viewed in the context of the petrogenesis of the mare basalt sources because the wide compositional variation observed in the basalt suite indicates that they represent a highly diverse group of mantle sources. Specifically, many basalts have high Mg-olivine, indicating their sources formed early in the LMO solidification sequence (e.g., Shearer et al., 2006; Snyder et al., 1997). Some mare basalts have high Ti contents, indicating that they are derived from cumulates that formed after 85-90 percent solidification of the LMO (Snyder et al., 1992), whereas others are enriched in urKREEP that was produced after >99% solidification of the LMO (Warren and Wasson, 1979; Snyder et al., 1992). In addition, petrogenetic models of the basalt compositions indicate that many have assimilated anorthositic crustal rocks before erupting on the surface (Shearer and Papike, 1993; Neal et al., 1994; Snyder et al., 1997; Shearer et al., 2006). The linearity of Sm-Nd data in Fig. 7, therefore, indicates that equilibrium existed $4331^{+35}/_{-37}$ Ma ago on a very large scale between a suite of compositionally diverse mantle rocks and crustal assimilants.

Even clearer evidence for isotopic equilibrium between the lunar crust and mantle at this time is derived from the observation that the mare basalt ^{146}Sm-^{142}Nd isotopic data are indistinguishable from data we previously measured on mineral fractions from FAS crustal cumulates (Fig. 7). Data for FAS samples 60025 (Borg et al., 2011), 60016 (Marks et al., 2014b), and 62237 (Sio and Borg, 2018) are presented in the Supplementary Material. Data for noritic anorthosites 60025 and 60016 are directly comparable to the mare basalt data because both were generated using identical mass spectrometry techniques and isotopic tracers. Furthermore, these FAS samples require no correction for neutron capture. In contrast, the Sm-Nd data for troctolitic anorthosite 62237 require

correction for the capture of thermal neutrons that was completed using the measured Sm isotopic composition of the rock and the relationship depicted in Fig. 5. Although the 62237 mineral fractions yielded lower amounts of Sm and Nd than 60016 and 60025, resulting in larger uncertainties (Sio and Borg, 2018), the data lie within error of the isochron defined by the other FAS cumulate samples and the mare basalts. In fact, all the Sm-Nd data from the basalts and anorthosites that we have analyzed define a single isochron with a slope corresponding to an age of $4336^{+31}/_{-32}$ Ma. This age appears to record the when the mare basalt sources and FAS cumulate samples formed from a common isotopic reservoir.

7. Discussion

7.1. Sm-Nd isotopic equilibrium

Identical Sm-Nd isotopic systematics of the mare basalt source regions and FAS crustal cumulates (Fig. 7) require these materials to be produced from a common precursor reservoir at the same time. This reservoir was likely to be global, or nearly global, in scale because the samples are from locations that are separated by almost 2000 km (Fig. 1) and originate from a variety of depths (Longhi, 1992; Shearer and Papike, 1993; McCallum and O'Brien, 1996; Shearer et al., 2006). The volume of the Moon represented by the samples used to define the isochron (Fig. 7) is calculated using the area between the Apollo landing sites and the estimated depths of formation of the mare basalt sources and FAS cumulates. Ferroan anorthosite suite cumulates are estimated to have crystallized around 20 km depth (McCallum and O'Brien, 1996), whereas the mare basalt sources are thought to have solidified somewhere between 300 to 1000 km depth. The total volume of the Moon represented by the sample suite on Fig. 7 is approximately 0.8, 1.0, or 2.9 percent depending on whether the depth of the mare basalt sources are assumed to be 300 km (Shearer and Papike, 1993), 400 km (Shearer et al., 2006) or 1000 km (Longhi, 1992), respectively. Note that this represents a minimum volume because the samples defining the isochron were collected over a limited area on the lunar nearside. A significantly larger volume of the Moon was probably in isotopic equilibrium at 4.34 Ga given the fact that every sample we have analyzed, including meteorite samples from unknown lunar locations, fall on the isochron.

7.2. Significance of lunar ^{146}Sm-^{142}Nd isochron

The formation of rocks in isotopic equilibrium over thousands of kilometers distance places important constraints on potential mechanisms for their production. Critically, isotopic equilibrium at 4.34 Ga requires that the FAS crustal cumulates and mare basalt sources were derived from a common reservoir, with homogeneous radiogenic isotopic compositions (i.e. ^{142}Nd/^{144}Nd and ^{143}Nd/^{144}Nd ratios), at the same time. Although the Sm-Nd isotopic system remains open at temperatures near 850 °C on a scale defined by distances at which Sm and Nd can diffuse (McCallum et al., 2006), diffusion will not result in isotopic equilibrium on the kilometer scale. Thus, to maintain or re-establish Sm-Nd isotopic equilibrium, a huge portion of the body must have been molten. Elemental fractionation of Sm and Nd documented by the isochron, therefore, records the time of liquid/crystal partitioning associated with crystallization.

Like all isochrons, the geologic significance of the Sm-Nd model age depends on the nature of the geologic event that produced the mare basalt sources and FAS crustal cumulates. There are three general scenarios that might account for global-scale isotopic equilibrium on the Moon relatively late in Solar System history. First, Sm-Nd re-equilibration of a solid Moon could result from widespread melting in response to mantle overturn or a very large impact occurring near 4.34 Ga. Second, the young age might reflect delayed differentiation of the LMO due to the presence of an additional heat source that keeps a large portion of the Moon molten until 4.34 Ga. Finally, the 4.34 Ga age could reflect rapid cooling and differentiation of the magma ocean late in Solar System history. Note that re-equilibrium of the Moon and delayed cooling of the LMO, scenarios 1 and 2, are consistent with formation of the Moon as early as ~4.56 Ga, whereas scenario 3 implies that the Moon formed relatively late in Solar System history. The 4.34 Ga Sm-Nd isochron age can, therefore, be inferred to record different events depending on which of these scenarios is considered. For example, if the Sm-Nd isotopic systematics reflect rapid solidification of the LMO, then the age closely approximates the time of accretion following the Giant Impact. On the other hand, if the Moon remained molten for a few hundred million years, then the Sm-Nd isochron would not approximate the age of accretion, but instead reflect the time of accretion plus the duration of time the Moon remained molten. Finally, if the Moon was heated significantly after it formed, the Sm-Nd age would record the time when it again cooled and then differentiated for a second time. Below we discuss the feasibility of these scenarios to produce rocks in isotopic equilibrium over a vast area of the Moon.

7.3. Secondary melting of LMO cumulates

Overturn of primordial cumulates that formed during crystallization of the magma ocean was initially postulated by Ringwood and Kesson (1976). These authors noted that late formed LMO cumulates that were produced near the top of the cumulate pile, are expected to be rich in Fe and Ti, and have a relatively high density of ~3.75 g/cm^3, whereas early-formed cumulates at the base of the cumulate pile would be rich in Mg and a have a much lower density near 3.30 g/cm^3. Ringwood and Kesson (1976) speculated that the density differences between the early- and late-formed LMO cumulates led to convective overturn of the cumulate pile. Borg et al. (2011) suggested that overturn might, in turn, lead to localized melting during convection that could result in at least partial re-equilibration of the lunar mantle. However, the global-scale isotopic equilibrium observed in Fig. 7 is inconsistent with density-driven overturn because this would not result in isotopic equilibrium between the mantle and crust as required by the Sm-Nd isochron. This stems from the fact that a plagioclase-rich crust, with a density of approximately 2.59 to 2.87 g/cm^3 (Huang and Wieczorek, 2012), would remain buoyant during overturn of the more dense underlying mafic cumulates.

It has also been suggested that the Sm-Nd isotopic systematics of the mare basalts reflect heating associated with a very large impact (McLeod et al., 2014). Isotopic equilibrium on such a global-scale is inconsistent with localized impact melting occurring substantially after LMO solidification because this process is not expected to result in melting of a large portion of both the mantle and crust. The fact that all of the mare basalt and anorthosite data lie within uncertainty of the isochron indicates that any isotopic heterogeneity that existed in hypothetical crustal or mantle protoliths prior to the formation of the mare basalt sources and FAS cumulates has been erased. As noted above, for an impact to produce the isotopic equilibrium observed in the lunar rock suite, the impact would need to completely melt the original source rocks to a depth ranging from 300 km, to perhaps as much as 1000 km. This reflects the fact that physical mixing of the radiogenic Nd isotopes in the target lithologies is required. Such a large impact, although not impossible, is improbable.

7.4. Delayed cooling of the LMO

Simple slow cooling of the LMO cannot account for the relatively young Sm-Nd model age either. This stems from the fact that progressive solidification of LMO cumulates over an extended period of time would result in significant scatter on the Sm-Nd isochron. For example, a source region with a present-day $^{147}Sm/^{144}Nd$ ratio of 0.28, that formed at 4.5 Ga from an undifferentiated Moon, would have a $^{142}Nd/^{144}Nd$ ratio that is ~40 ppm above the Sm-Nd isochron. In fact, a hypothetical mare basalt source forming more than ~50 Ma before or after 4.34 Ga would be manifest by a point that fell off the isochron in Fig. 7. Thus, the only cooling scenario that could account for the young Sm-Nd isochron age is one in which a significant portion of the Moon remained molten for an extended period of time after it accreted. However, thermal models produced by Elkins-Tanton et al. (2011) suggest that ~80% of the Moon should solidify within a few thousand years and the remainder would solidify within a few million years. These models therefore imply that additional sources of heat are required to extend the duration of cooling by tens to hundreds of millions of years. One such source is tidal heating from the Earth (e.g., Garrick-Bethell et al., 2010; Meyer et al., 2010). Another is asymmetric distribution of heat producing elements in the lunar interior (Shearer et al., 2006). Although these heating processes might extend the duration of cooling up to ~200 Ma, they are unlikely to generate Sm-Nd isotopic systematics observed in the FAS crustal cumulates and the mare basalt sources. This stems from the observation that these models do not predict generation of enough heat to maintain a molten reservoir of the size required by the Sm-Nd isochron. Thus, neither prolonged or delayed cooling of the LMO is a viable mechanism to account for the Sm-Nd isotopic systematics observed in Fig. 7, unless a heat source with enough energy to keep the Moon molten to depths of 300 to 1000 km is found.

7.5. Primordial solidification of the LMO

The final possibility is that the Sm-Nd isotopic equilibrium observed between various mantle reservoirs and the crust was inherited from primordial solidification of the LMO. One appealing aspect of this scenario is that it accounts for the observation that the Sm-Nd model age is concordant with ages determined on rocks that have been argued to represent crystallization products of the LMO. For example, recent age determinations of FAS cumulate samples based on the long-lived ^{147}Sm-^{143}Nd isotopic system are concordant with the ^{146}Sm-^{142}Nd isochron age presented here. Specifically, ages of 4367 ± 11 Ma, 4302 ± 28 Ma, and 4359 ± 65 Ma have been determined for ferroan noritic and troctolitic anorthosites 60025 (Borg et al., 2011), 60016 Clast 3A (Marks et al., 2014b), and 62237 (Sio and Borg, 2018), respectively. The young ^{146}Sm-^{142}Nd isochron age defined by the mare basalts and FAS mineral separates is also concordant with ages determined on urKREEP, which is another lunar lithology argued to represent primordial solidification products of the LMO. Model ages for the formation of urKREEP are 4353 ± 37 Ma, 4389 ± 45 Ma (Gaffney and Borg, 2014), 4.39 ± 0.04 Ga (Sprung et al., 2013), 4.42 ± 0.07 Ga (Nyquist and Shih, 1992), and 4.33 ± 0.08 Ga (Carlson and Lugmair, 1981) yielding an average of 4382 ± 54 Ma. Thus, ages independently determined on different suites of rocks deemed to represent LMO cumulates are concordant within uncertainty as predicted by the LMO model of lunar differentiation. Finally, the absence of isotopic variability in the short lived ^{182}Hf-^{182}W system in lunar samples is consistent with solidification of the LMO after 4.5 Ga (Touboul et al., 2015; Kruijer and Kleine, 2017).

This scenario does not permit lunar rocks to be older than about 4.38 Ga despite the fact that several investigations have measured such ages. However, some of the oldest age estimates for FAS cumulate samples, such as 67016 (4573 ± 160 Ma; Alibert et al., 1994) and 67215 (4408 ± 130 Ma; Norman et al., 2003), have large uncertainties and MSWD's in excess of 6 (Borg et al., 2015). Other published old FAS sample ages, such as the 4437 ± 39 Ma age determined on 60025 by Carlson and Lugmair (1988), have not been reproduced by more recent studies (Borg et al., 2011). Likewise, Barboni et al. (2017) reported a model age of >4.51 Ga calculated for the formation of urKREEP that is older than 4.38 Ga. However, this age is not only older than the maximum age permitted by the ^{182}Hf-^{182}W system (Touboul et al., 2015; Kruijer and Kleine, 2017), the Hf isotopic systematics of the zircons are significantly different that those observed for other KREEP-rich samples (Sprung et al., 2013; Gaffney and Borg, 2014).

This illustrates the dilemma facing the lunar chronology community in which the validity of individual age determinations must be weighed against the apparent coherence of ages defined for various lunar lithologies using a range of analytical approaches. It is complicated by the fact that ancient lunar samples have experienced significant amounts of thermal metamorphism and often contain very low abundances of elements that constitute radiogenic chronometers, making them extremely difficult to date reliably. Nevertheless, there is a clear preponderance of lunar ages around 4.35 Ga (Borg et al., 2015). On one hand this might represent a secondary pulse of magmatism that followed primordial differentiation, whereas on the other this could represent primordial differentiation itself. Traditionally, which of these possibilities is deemed to be valid largely depends on the reliability assigned to the most ancient ages. The Sm-Nd data presented here provide an additional constraint. Specifically, that the mechanism that is responsible for the widespread distribution of ~4.35 Ga ages on the Moon must also result in Sm-Nd isotopic equilibrium throughout the mantle and crust at that time. A model in which the LMO cools rapidly and late in Solar System history seems to satisfy these criteria most easily.

7.6. Nd isotopic composition of the Moon

The initial epsilon ^{142}Nd isotopic composition determined from the y-intercept of the isochron in Fig. 7 records the bulk $^{142}Nd/^{144}Nd$ isotopic composition of the Moon provided the samples that define the isochron are indeed representative of solidification products of the LMO. The initial epsilon ^{142}Nd value determined from this isochron is 15 ± 5 ppm lower than the values estimated for bulk Earth (defined as 0 ppm), but very similar to the average of eight ordinary chondrites (−18 ± 5 ppm) and eleven enstatite chondrites (−10 ± 3 ppm) that we have previously measured (Burkhardt et al., 2016). Difference in the apparent epsilon ^{142}Nd value of Earth and Moon were previously noted by Rankenburg et al. (2006) and were attributed to analytical artifacts associated with differences in neutron capture corrections and mass spectrometry analytical routines (static versus dynamic acquisition) used to measure the Nd isotopic compositions of the samples (Brandon et al., 2009). These mechanisms, however, are unlikely to account for the differences we measure for Earth, Moon, and chondritic meteorites because all measurements were completed using the same dynamic acquisition routine. Furthermore, most of the lunar samples analyzed here have very small neutron capture corrections on $^{142}Nd/^{144}Nd$ (Fig. 4) and those samples that do require significant corrections are indistinguishable from the uncorrected measurements. The difference between the Nd isotopic composition of the Earth and Moon is also unlikely to reflect nucleosynthetic processes because both bodies have similar Nd, Cr, Ti, W, and O isotopic compositions (see Supplementary Material; Lugmair and Shukolyukov, 1998; Zhang et al., 2012; Touboul et al., 2015; Kruijer et al., 2015; Wiechert et al., 2001;

Young et al., 2016). Instead the difference in Nd isotopic composition likely reflects derivation of the Earth and Moon from reservoirs with different Sm/Nd ratios. Specifically, the Moon must have a lower Sm/Nd ratio than the Earth. One possibility is that the difference reflects Sm/Nd elemental fractionation in the proto-Earth that was inherited by the Moon during the Giant Impact. Alternatively, the Sm/Nd of the bulk Earth calculated from measured $^{142}Nd/^{144}Nd$ ratios could be inaccurate because there is a hidden terrestrial reservoir that is characterized by very low Sm/Nd (Boyet and Carlson, 2005).

8. Conclusion

High precision Sm-Nd isotopic measurements have been completed on a suite of mare basalts and compared to data previously obtained on FAS crustal cumulate samples. The basalt samples were selected because they represent the largest geographical area sampled from the Moon and span the widest known compositional variation. The Sm-Nd isotopic systematics of the samples were corrected for the effects of both thermal and epithermal neutron capture based on their measured Hf and Sm isotopic compositions, as well as their rare earth element abundances, using the model of Gaffney and Borg (2014). The $^{147}Sm/^{144}Nd$ of the basalt source regions were calculated from their measured $^{147}Sm/^{144}Nd$ and $^{143}Nd/^{144}Nd$ ratios and crystallization ages. A $^{147}Sm/^{144}Nd$-$^{142}Nd/^{144}Nd$ whole rock isochron defined by all 30 basalt source regions defines an age of $4331^{+35}/_{-37}$ Ma. This is in excellent agreement with previous investigations based on more limited datasets (Nyquist et al., 1995; Rankenburg et al., 2006; Boyet and Carlson, 2007; Brandon et al., 2009; McLeod et al., 2014). The analytical uncertainty associated with the isochron presented here incorporates both the uncertainty associated with the regression and the uncertainty associated with the ^{146}Sm half-life. Whole rocks and mineral fractions derived from three FAS crustal samples fall on the Sm-Nd isochron defined by the mare basalt source regions, indicating that both rock suites formed from the same reservoir, contemporaneously. A slightly more precise age of $4336^{+31}/_{-32}$ Ma is obtained using all of the data for both the basalt sources and FAS samples. The mare basalt source regions and FAS samples that define the Sm-Nd isochron are from all Apollo landing sites, except Apollo 14, and have estimated crystallization depths spanning a minimum depth of ~20 km to a maximum of 300 km, to perhaps as deep as 1000 km. This implies that a minimum of 1-3% of the entire volume of the Moon was in Sm-Nd isotopic equilibrium at ~4.34 Ga.

The Sm-Nd isotopic equilibrium observed in the lunar sample suite collected over several thousand kilometers distance and derived from several hundred kilometers depths requires a very large portion of the Moon to have been molten around 4.34 Ga. Localized melting, or heating below the liquidus temperature of the bulk Moon, will not result in global scale Sm-Nd isotopic equilibrium over hundreds of kilometers distance. The most viable mechanism to account for global-scale melting of the Moon is initial accretion. The magma ocean model of lunar differentiation, originally developed to account for the geologic and geochemical diversity of lunar rocks, predicts the observed global-scale Sm-Nd isotopic equilibrium. Thus, the most conservative interpretation of the Sm-Nd model age is that it records the solidification of the LMO.

Acknowledgements

This work was performed under the auspices of the U.S. Department of Energy by Lawrence Livermore National Laboratory under Contract DE-AC52-07NA27344. This work was supported by NASA Cosmochemistry and Emerging Worlds grants NNH12AT84I and NNH16AC441 (LEB), Solar System Workings grant NNH13AW501 (AMG), and Laboratory Directed Research and Development grant 17-ERD-001 (LEB). The authors are grateful for detailed reviews from Dr. Richard Carlson and Dr. Jim Connelly, and comments and suggestions from Associate Editor Dr. Frederic Moynier.

Appendix A. Supplementary material

Supplementary material related to this article can be found online at https://doi.org/10.1016/j.epsl.2019.07.008.

References

Alibert, C., Norman, M.D., McCulloch, M.T., 1994. An ancient age for a ferroan anorthosite clast from lunar breccia 67016. Geochim. Cosmochim. Acta 58, 2921–2926. https://doi.org/10.1016/0016-7037(94)90125-2.

Barboni, M., Boehnke, P., Keller, B., Kohl, I.E., Schone, B., Young, E.D., McKeegan, K.D., 2017. Early formation of the Moon 4.51 billion years ago. Sci. Adv. 3, e1602365. https://doi.org/10.1126/sciadv.1602365.

Borg, L.E., Brennecka, G.A., Symes, S.J.K., 2016. Accretion timescale and impact history of Mars deduced from the isotopic systematics of martian meteorites. Geochim. Cosmochim. Acta 175, 150–167. https://doi.org/10.1016/j.gca.2015.12.002.

Borg, L.E., Gaffney, A.M., Shearer, C.K., 2015. A review of lunar chronology revealing a preponderance of 4.34–4.37 Ga ages. Meteorit. Planet. Sci. 50, 715–732. https://doi.org/10.1111/maps.12373.

Borg, L.E., Connelly, J.N., Boyet, M., Carlson, R.W., 2011. Evidence that the Moon is either young or did not have a global magma ocean. Nature 477, 70–72. https://doi.org/10.1038/nature10328.

Boyet, M., Carlson, R.W., 2007. A highly depleted moon or a non-magma ocean origin for the lunar crust? Earth Planet. Sci. Lett. 262, 505–516. https://doi.org/10.1016/j.epsl.2007.08.009.

Boyet, M., Carlson, R.W., 2005. ^{142}Nd evidence for early (>4.53 Ga) global differentiation of the silicate Earth. Science 309, 576–581. https://doi.org/10.1126/science.1113634.

Brandon, A.D., Lapen, T.J., Debaille, V., Beard, B.L., Rakenburg, K., Neal, C.R., 2009. Evolution and bulk Sm/Nd of the Moon. Geochim. Cosmochim. Acta 73, 6421–6445.

Burkhardt, C., Borg, L.E., Brennecka, G.A., Shollenberger, Q.R., Dauphas, N., Kleine, T., 2016. A nucleosynthetic origin for the Earth's anomalous ^{142}Nd composition. Nature 537, 394–398. https://doi.org/10.1038/nature18956.

Carlson, R.W., Lugmair, G.W., 1988. The age of ferroan anorthosite 60025: oldest crust on a young Moon? Earth Planet. Sci. Lett. 90, 119–130. https://doi.org/10.1016/0012-821X(88)90095-7.

Carlson, R.W., Lugmair, G.W., 1981. Sm-Nd age of lherzolite 67667: implications for the processes involved in lunar crustal formation. Earth Planet. Sci. Lett. 56, 1–8. https://doi.org/10.1016/0012-821X(81)90112-6.

Connelly, J.N., Bizzarro, M., Krot, A.N., Nordlund, A., Wielandt, D., Ivanova, M.A., 2012. The absolute chronology and thermal processing of solids in the solar protoplanetary disk. Science 338, 651–655. https://doi.org/10.1126/science.1226919.

Connelly, J.N., Ulfbeck, D.G., Thrane, K., Bizzarro, M., Housh, T.A., 2006. Method for purifying Lu and Hf for analyses by MC-ICP-MS using TODGA resin. Chem. Geol. 233, 126–136. https://doi.org/10.1016/j.chemgeo.2006.02.020.

Elkins Tanton, L.T., Burgess, S., Yin, Q.-Z., 2011. The lunar magma ocean: reconciling the solidification process with lunar petrology and geochronology. Earth Planet. Sci. Lett. 304, 326–336. https://doi.org/10.1016/j.epsl.2011.02.004.

Gaffney, A.M., Borg, L.E., 2014. A young solidification age for the lunar magma ocean. Geochim. Cosmochim. Acta 140, 227–240. https://doi.org/10.1016/j.gca.2014.05.028.

Garrick-Bethell, I., Nimmo, F., Wieczorek, M.A., 2010. Structure and formation of the lunar farside highlands. Science 330, 949–951. https://doi.org/10.1126/science.1193424.

Hartmann, W.K., Davis, D.R., 1975. Satellite-sized planetesimals and lunar origin. Icarus 24, 504–515. https://doi.org/10.1016/0019-1035(75)90070-6.

Huang, Q., Wieczorek, M.A., 2012. Density and porosity of the lunar crust from gravity and topography. J. Geophys. Res. 117, E05003. https://doi.org/10.1029/2012JE004062.

Kinoshita, N., Paul, M., Kashiv, Y., Collon, P., Deibel, C.M., DiGiovine, B., Greene, J.P., Henderson, D.J., Jiang, C.L., Marley, S.T., Nakanishi, T., Pardo, R.C., Rehm, K.E., Roberston, D., Scott, R., Schmitt, C., Tang, X.D., Vondrasek, R., Yokoyama, A., 2012. A shorter ^{146}Sm half-life measured and implications for ^{146}Sm–^{142}Nd chronology in the Solar System. Science 335, 1614–1617. https://doi.org/10.1126/science.1215510.

Kruijer, T.S., Kleine, T., 2017. Tungsten isotopes and the origin of the Moon. Earth Planet. Sci. Lett. 475, 15–24. https://doi.org/10.1016/j.epsl.2017.07.021.

Kruijer, T.S., Kleine, T., Fischer-Godde, M., Sprung, P., 2015. Lunar tungsten isotopic evidence for the late veneer. Nature 520, 534–537. https://doi.org/10.1038/nature14360.

Lugmair, G.W., Shukolyukov, A., 1998. Early solar system timescales according to ^{53}Mn-^{53}Cr systematics. Geochim. Cosmochim. Acta 56, 1673–1694. https://doi.org/10.1016/S0016-7037(98)00189-6.

Longhi, J., 1992. Experimental petrology and petrogenesis of mare volcanics. Geochim. Cosmochim. Acta 56, 2235–2252. https://doi.org/10.1016/0016-7037(92)90186-M.

Marks, N.E., Borg, L.E., Hutcheon, I.D., Jacobsen, B., Clayton, R.N., 2014a. Samarium-neodymium chronology of an Allende calcium-aluminum-rich inclusion with implications for ^{146}Sm isotopic evolution. Earth Planet. Sci. Lett. 405, 15–24. https://doi.org/10.1016/j.epsl.2014.08.017.

Marks, N.E., Borg, L.E., Gaffney, A.M., Shearer, C.K., Burger, P., 2014b. Additional evidence for young ferroan anorthositic magmatism on the Moon from Sm-Nd isotopic measurements if 60016 Clast 3A. In: 45th Lunar Planet. Sci Conf. Abstr. #1129.

McCallum, S., Domeneghetti, M.C., Schwartz, J.M., Mullen, E.K., Zema, M., Cámara, F., McCammon, C., Ganguly, J., 2006. Cooling history of lunar Mg-suite gabbronorite 76255, troctolite 76535 and Stillwater pyroxenite SC-936: the record in exsolution and ordering in pyroxenes. Geochim. Cosmochim. Acta 70, 6068–6078. https://doi.org/10.1016/j.gca.2006.08.009.

McCallum, I.S., O'Brien, H.E., 1996. Stratigraphy of the lunar highland crust: depths of burial of lunar samples from cooling-rate studies. Am. Mineral. 81, 1166–1175. https://doi.org/10.2138/am-1996-9-1015.

McLeod, C., Brandon, A.D., Armytage, R.M.G., 2014. Constraints in the formation age and evolution of the Moon from ^{142}Nd-^{143}Nd systematics of Apollo 12 basalts. Earth Planet. Sci. Lett. 396, 179–189. https://doi.org/10.1016/j.epsl.2014.04.007.

Meissner, F., Schmidt-Ott, W.-D., Ziegeler, L., 1987. Half-life and alpha-ray energy of ^{146}Sm. Z. Phys. A 327, 171–174. https://doi.org/10.1007/BF01292406.

Meyer, J., Elkins-Tanton, L., Wisdom, J., 2010. Coupled thermal-orbital evolution of the early Moon. Icarus 208, 1–10. https://doi.org/10.1016/j.icarus.2010.01.029.

Neal, C.R., Hacker, M.D., Snyder, G.A., Taylor, L.A., 1994. Basalt generation at the Apollo 12 site, part 1: new data, classification, and re-evaluation. Meteorit. Planet. Sci. 29, 334–348. https://doi.org/10.1111/j.1945-5100.1994.tb00597.

Norman, M.D., Borg, L.E., Nyquist, L.E., Bogard, D.D., 2003. Chronology, geochemistry, and petrology of a ferroan noritic anorthosite clast from Descartes breccia 67215: clues to the age, origin, structure, and impact history of the lunar crust. Meteorit. Planet. Sci. 38, 645–661. https://doi.org/10.1111/j.1945-5100.2003.tb00031.

Nyquist, L.E., Wiesmann, H., Bansal, B.M., Shih, C.-Y., Keith, J.E., Harper, C.L., 1995. ^{146}Sm-^{142}Nd formation interval for the lunar mantle. Geochim. Cosmochim. Acta 59, 2817–2837. https://doi.org/10.1016/0016-7037(95)00175-Y.

Nyquist, L.E., Shih, C.-Y., 1992. The isotopic record of lunar volcanism. Geochim. Cosmochim. Acta 56, 2213–2234. https://doi.org/10.1016/0016-7037(92)90185-L.

Rankenburg, K., Brandon, A.D., Neal, C.R., 2006. Neodymium isotope evidence for chondritic composition of the Moon. Science 312, 1369–1372. https://doi.org/10.1126/science.1126114.

Ringwood, A.E., Kesson, S.E., 1976. A dynamic model for mare basalt petrogenesis. In: Proc. 7th Lunar Planet. Sci. Conf., pp. 1697–1722.

Shearer, C.K., Hess, P.C., Wieczorek, M.A., Pritchard, M.E., Parmentier, M.E., Borg, L.E., Longhi, J., Elkins-Tanton, L.T., Neal, C.R., Antonenko, A., Canup, R.M., Halliday, A.N., Grove, T.L., Hager, B.H., Lee, D.C., Wiechert, U., 2006. Thermal and magmatic evolution of the Moon. In: Jolliff, B.L., Wieczorek, M.A., Shearer, C.K., Neal, C.R. (Eds.), New Views of the Moon. In: Reviews in Mineralogy and Geochemistry, vol. 60, pp. 365–518. Chapter 4.

Shearer, C.K., Papike, J.J., 1993. Basalt magmatism on the Moon: a perspective from volcanic glass beads. Geochim. Cosmochim. Acta 57, 4785–4812. https://doi.org/10.1016/0016-7037(93)90200-G.

Sio, C.K., Borg, L.E., 2018. Sm-Nd isotopic systematics of ferroan anorthosite (FAN) 62237: evidence for co-magmatism of FANs at 4.36 Ga. In: 49th Lunar Planet. Sci. Conf. Abstr. #2083.

Smith, J.V., Anderson, A.T., Newton, R.C., Olsen, E.J., Wyllie, P.J., 1970. Petrologic history of the Moon inferred from petrography, mineralogy, and petrogenesis of Apollo 11 rocks. In: Proc. 1st Lunar Sci. Conf., pp. 897–925.

Snyder, G.A., Neal, C.R., Taylor, L.A., Halliday, A.N., 1997. Anatexis of lunar cumulate mantle in time and space: clues from trace-element, strontium, and neodymium chemistry if parental Apollo 12 basalts. Geochim. Cosmochim. Acta 61, 2731–2747. https://doi.org/10.1016/S0016-7037(97)00082-3.

Snyder, G.A., Taylor, L.A., Neal, C.R., 1992. A chemical model for generating the source of mare basalts: combined equilibrium and fractional crystallization of the lunar magmasphere. Geochim. Cosmochim. Acta 56, 3809–3823. https://doi.org/10.1016/0016-7037(92)90172-F.

Sprung, P., Kleine, T., Scherer, E.E., 2013. Isotopic evidence for chondritic Lu/Hf and Sm/Nd of the Moon. Earth Planet. Sci. Lett. 380, 77–87. https://doi.org/10.1016/j.epsl.2013.08.018.

Sprung, P., Scherer, E.E., Upadhyay, D., Leya, I., Mezger, K., 2010. Non-nucleosynthetic heterogeneity in non-radiogenic stable Hf isotopes: implications for early solar system chronology. Earth Planet. Sci. Lett. 295, 1–11. https://doi.org/10.1016/j.epsl.2010.02.050.

Touboul, M., Puchtel, I.S., Walker, R.J., 2015. Tungsten isotopic evidence for disproportional late accretion to the Earth and Moon. Nature 520, 530–533. https://doi.org/10.1038/nature14355.

Warren, P.H., Wasson, J.T., 1979. The origin of KREEP. Rev. Geophys. Space Phys. 17, 73–88. https://doi.org/10.1029/RG017i001p00073.

Wiechert, U., Halliday, A.N., Lee, D.-C., Snyder, G.A., Taylor, L.A., Rumble, D., 2001. Oxygen isotopes and the Moon-forming giant impact. Science 294, 345–348. https://doi.org/10.1126/science.1063037.

Wood, J.A., Dickey, J.S., Marvin, U.B., Powell, B.N., 1970. Lunar anorthosites and a geophysical model of the Moon. In: Proc. 1st Lunar Sci. Conf., pp. 965–988.

Young, E.D., Kohl, I.E., Warren, P.H., Rubie, D.C., Jacobsen, S.A., Morbidelli, A., 2016. Oxygen isotopic evidence for vigorous mixing during the Moon-forming giant impact. Science 351, 493–496. https://doi.org/10.1126/science.aad0525.

Zhang, J., Dauphas, N., Davis, A.M., Leya, I., Fedkin, A., 2012. The proto-Earth as a significant source of lunar material. Nat. Geosci. 5, 251–255. https://doi.org/10.1038/ngeo1429.